Contents list available at IJRED website

International Journal of Renewable Energy Development

Journal homepage: https://ijred.undip.ac.id

Research Article

Synthesis of Al-Y doped-lithium lanthanum zirconate and the effect of cold isostatic pressure to its electrical properties

Fitria Rahmawati*, Septia K. Arifah, Yuniawan Hidayat

Research Group of Solid-State Chemistry & Catalysis, Chemistry Department, Sebelas Maret University, Jl. Ir. Sutami 36 A Kentingan, Surakarta 57126, Indonesia

Abstract. This research aims to study the Al-Y dopant to Lithium Lanthanum Zirconate (LLZO) to the characteristics and electrical properties of the LLZO as solid electrolyte. The synthesis was conducted through solid state reaction with Al_2O_3 and Y_2O_3 as dopant precursors. X-ray diffraction analysis along with Le Bail refinement was done to understand their structure, and phase content inside. The result found that Al and Y doping increased the cubic phase from 49.58% to 84.91%. The Al-Y doped-LLZO (LLZAYO) powder was then treated by a various cold isostatic pressing, CIP of 0, 20, 30, and 40 MPa to understand the effect of cold isostatic pressure to the ionic conductivity and solid electrolyte performance of the material even without heat sintering treatment. The result found that the green pellet of LLZAYO) which was isostatically pressed by 40 MPa at room temperature provides (9.06 ±0.26) x10^{-6} Scm^{-1}, about 8 times higher than the LLZO without doping, i.e., (1.25 ±0.01) x 10^{-6} Scm^{-1}. All solid-state battery with the prepare LLZAYO CIP 40 as solid electrolyte shows reversible reaction of Li/Li^+ redox accompanied with Al/Al^{3+} redox. The Al/Al^{3+} reaction seems to decrease the electronic resistance between LCO-LLZAYO CIP40-Li which causes the full cell performance to decrease. The initial specific charging capacity is 82 mAh/g, and the initial discharge was 83 mAh/g, confirming 101 % of Coulombic efficiency. The discharge capacity drops to 46 mAh/g at second cycle, leading to a decrease in Coulombic efficiency to 56 %.

Keywords: lithium lanthanum zirconate, aluminium dopant; yttrium dopant; all solid-state lithium-ion battery

Received: 21st April 2023; Revised: 24nd June 2023; Accepted: 5th July 2023; Available online: 10th July 2023

1. Introduction

Recently, electricity storage device is essential for several electronic devices, in which Lithium-Ion Batteries (LIBs) are successfully dominate the market due to the long service life, and high specific energy density (Li *et al.*, 2015). The liquid electrolyte used in LIBs provides good ionic mobilities (Hwang *et al.*, 2018). However, some problems were revealed, including liquid leakage, explosion, and fire risk (Chen *et al.*, 2018). Solid electrolyte, SE, is an alternative to overcome the difficulties because of eliminating potential leakage, explosion, and fire risk. Some solid electrolytes for all-solid-state lithium-ion battery (ASSB) have been investigated, including lithium lanthanum titanate, LLTO (Inaguma *et al.*, 2004), lithium titanate (Priyono *et al.*, 2017), lithium lanthanum zirconate (LLZO) (Awaka *et al.*, 2009), lithium phosphorus sulfide (Hayashi *et al.*, 2010), lithium sulfide- phosphorus sulfide (Mizuno *et al.*, 2005), glassy ceramic Li_2S-P_2S_5 (Mizuno *et al.*, 2005) and $Li_2P_3S_{11}$ (Hayashi *et al.*, 2010).

To increase the ionic conductivity, some researchers modified the electrolyte such as by adding 2% of LiF into $Li_{6.5}La_3Zr_{1.5}Ta_{0.5}O_{12}$ (LLZTO) to produce LLZT-2LiF (Li *et al.*, 2017), doped Ga to produce $Li_{6.4}Ga_{0.2}La_3Zr_2O_{12}$(Chen et al., 2021), and combining $Li_{1.3}Al_{0.3}Ti_{1.7}(PO_4)_3$(LATP) with $Li_7La_3Zr_2O_{12}$ (LLZO)(Hung and Mohanty, 2023). The LiF addition decreases the interface resistance from 966 Ωcm^{-2} to 345 Ωcm^{-2} for LLZT and LLZT-2LiF, respectively(Li et al., 2017). Another researcher developed a solid electrolyte of $Li_7P_3S_{11}$, and combined it with MoS_2, and then used the composite of $MoS_2/Li_7P_3S_{11}$ as an ASSB electrode providing a reversible capacity of 547.1 $mAhg^{-1}$ under 60 cycles. However, the sulfide based-electrolyte is unstable under humidity and reacts with lithium metal anode to form a second phase (Takada, 2018).

Regarding chemical stability, lithium lanthanum zirconate $Li_7La_3Zr_2O_{12}$ (LLZO) is leading. LLZO is a garnet crystal type with a high ionic conductivity up to 10^{-3} Scm^{-1} (Awaka *et al.*, 2011). LLZO also has a wide voltage window between 0 to 6 Volt, low chemical reactivity with lithium electrodes, and air (Kim *et al.*, 2019; Qie *et al.*, 2012). The garnet LLZO could crystallize into a cubic structure, c-LLZO, and a tetragonal structure, t-LLZO. The tetragonal phase provides lower ionic conductivity than the cubic one, i.e., around 10^{-6} -10^{-7} Scm^{-1}, while cubic garnet provides around 10^{-3} to 10^{-4} Scm^{-1} (Li *et al.*, 2019). However, the synthesis of c-LLZO is not easy because of some factors, including composition of the precursors, the synthesis process, and the synthesis temperature, which strongly affect the result (Kokal *et al.*, 2011). To gain a fully cubic structure through solid-state reaction, a high temperature of 1230 °C for 36 h is required (Rettenwander *et al.*, 2014). Another previous research states that only heating at above 1180 °C would find a fully cubic structure. However, such a high temperature can cause a reaction with the alumina (Al_2O_3) crucible (Rangasamy *et al.*, 2012). Secondly, a high reaction

* Corresponding author
Email: fitria@mipa.uns.ac.id (F. Rahmawati)

https://doi.org/10.14710/ijred.2023.53901
ISSN: 2252-4940/© 2023.The Author(s). Published by CBIORE

temperature can cause Li decomposition and Li loss from the LLZO structure (Campanella *et al.*, 2021). Meanwhile, applying a temperature lower than 1180°C leads to a tetragonal structure of LLZO, which provides a lower ionic conductivity than a cubic structure (Kokal *et al.*, 2011). Therefore, modify the material, such as by doping an element into LLZO, can stabilizes the cubic structure, even though only low temperature and less time are applied for the LLZO treatment (Bernstein *et al.*, 2012; Rangasamy *et al.,* 2012). Some dopants for LLZO are Ga (Ghosh and Wasim Raja, 2022), Al (El-Shinawi *et al.*, 2017), and yttrium, Y (Bitzer *et al.,* 2016). The Al^{3+} which is introduced into the LLZO crystal structure during high-temperature sintering, will produces vacancies and then stabilize the cubic structure under room temperature. At least requires 0.204 mol Al^{3+} to stabilize the cubic structure (Rangasamy *et al.*, 2012). Meanwhile, Y^{3+} doping to LLZO was conducted by sol-gel method, in which the dry gel was calcined at a low temperature of 800°C for only 3 h. The synthesis time was fast but required much solvent, i.e., 281 mL of ethanol and 94 mL of methoxy ethanol. Hence, the result only provides 3.4 x 10^{-8} $S.cm^{-1}$(Bitzer *et al.*, 2016).

Considering the potential of Al to stabilizes the cubic structure, and provides a high ionic conductivity, meanwhile, the Y dopant provides fast reaction to stabilizes cubic structure, therefore this research combined the dual Al and Y doping. The doping was conducted through a solid-state reaction to prevent organic solvent use. The produced Y-Al doped-LLZO was analysed to understand its crystal structure and surface morphology. Various methods were applied to densify the Y-Al doped-LLZO pellet, including hot sintering, cold sintering, non-sintering, and a combination of cold sintering and isostatic pressure. Impedance measurement followed by Nyquist plot fitting analyses ionic conductivity of the prepared materials. Meanwhile, the solid electrolyte performance in a battery prototype was tested by cyclic voltammetry of full-cell $LiCoO_2$ - SE- Li metal.

2. Method

2.1. Synthesis of Y-Al doped-LLZO ($Li_{6.15}La_3Zr_{1.75}Y_{0.25}Al_{0.2}O_{11.75}$) (LLZAYO)

A stoichiometric amount of LiOH, La_2O_3, ZrO_2, Al_2O_3 and Y_2O_3 was thoroughly mixed in a ball mill for 12h, with zirconia balls as crusher and isopropanol as dispersant. The mixture powder was then dried, and was hydraulically pressed to produce a green pellet. the green pellet was then fired at 650 °C for 15 h, and the firing was continued to 1000 °C for 4 h producing LLZAYO. Similar method was done to produce $Li_7La_3Zr_2O_{12}$, LLZO, from LiOH, La_2O_3, and ZrO_2 as the precursors. To densify the LLZAYO pellet, the LLZAYO powder was pressed under 7 metric tons of pressure, and then followed by cold isostatic pressure (CIP) of 0, 20, 30, and 40 MPa to produce LLZAYO CIP-0, LLZAYO CIP-20, LLZAYO CIP-30, and LLZAYO CIP-40. All the prepared-materials were analysed with XRD equipped with Le Bail refinement (Rietica software, a free edition) to understand its crystal structure and phase content. The surface morphology was analysed by Scanning Electron Microscope (SEM), and a blocking method impedance analysis (EUCOL LCR Meter 20 Hz – 5 MHz) was done to investigate resistance and conductivity of the prepared-materials. The active electrode for blocking method was silver paste and silver wire. The impedance data was fitted with ZView software (CS Studio 5). The undoped-LLZO was also synthesized with the similar method for control.

2.2. Full cell of the solid electrolyte-electrodes

LLZAYO was polished until 1 mm thickness with sand paper No.500. $LiCoO_2$ (LCO) slurry was prepared by mix LCO powder with PVDF, NMP, and acetylene black at percentage ratio of 80:10:10 (Wang 2018). The mixture was stirred for 1 h. The slurry was then applied to LLZAYO pellet and was kept in argon glove box for 12 h, producing LLZAYO-LCO disk. To produce a full cell, Li metal was attached on the other side of the disk, by applying heat of 180 – 200°C in the argon glove box until the Li melted on it. Cu foil was attached on Li side, and Al foil was attached on LCO side. After being punched with crimping machine, the coin cell was ready for cyclic voltammetry analysis (Corrtest Electrochemical Workstation CS-150, scan rate 5 mVs^{-1}) to understand the electrochemical reaction within the full cell.

3. Result and discussion

XRD analysis to LLZAYO and LLZO, prepared in this research, resulted in diffraction patterns as described in Figure 1 compared with standard diffraction of c-LLZO and t-LLZO ICSD#422259 and ICSD#246816, respectively. The result shows that the LLZO produced in this research are crystallized within a cubic and tetragonal structure with a molar percentage of 49.58 % and 48.07 %, respectively. Le Bail refinement resulting plots as described in Figure 2, and the crystal structure and its molar percentage are listed in Table 1.

After Al and Y doping, the material was crystallized in cubic without the presence of tetragonal structure, and the molar percentage of cubic significantly increased to 84.91%. However, some secondary phases are still available, including trigonal $La(OH)_3$, monoclinic LaOOH, hexagonal La_2O_3, and monoclinic Y_2O_3 (Table 1). The availability of La_2O_3 and Y_2O_3 at 0.39 %mol and 12.32 % mol, respectively, indicate that the reaction did not completely proceed. Extending ball milling time over 12 h can facilitate complete reaction to produce a high purity result. Previous research on LLZO preparation, which applied twice of 12 h ball milling time even produced a single tetragonal structure, in which the Be-, or B-, or Zn- doping into LLZO also created a single tetragonal structure (Xiang et al., 2020). Another research to prepare LLZO through solid-state reaction with 2 h of mixer mill under a 20 Hz frequency found a

Table 1
The refinement result of LLZO and LLZAYO

Molar percentage (%)	materials	
	LLZO	LLZAYO
Cubic	**49.58**	**84.91**
tetragonal	48.07	-
trigonal $La(OH)_3$	0.78	1.36
Monoclinic ZrO_2	1.56	-
Monoclinic LaOOH	-	1.01
Hexagonal La_2O_3	-	0.39
Monoclinic Y_2O_3	-	12.32
Rp (%)	4.02	3.09
Rwp (%)	5.63	7.14

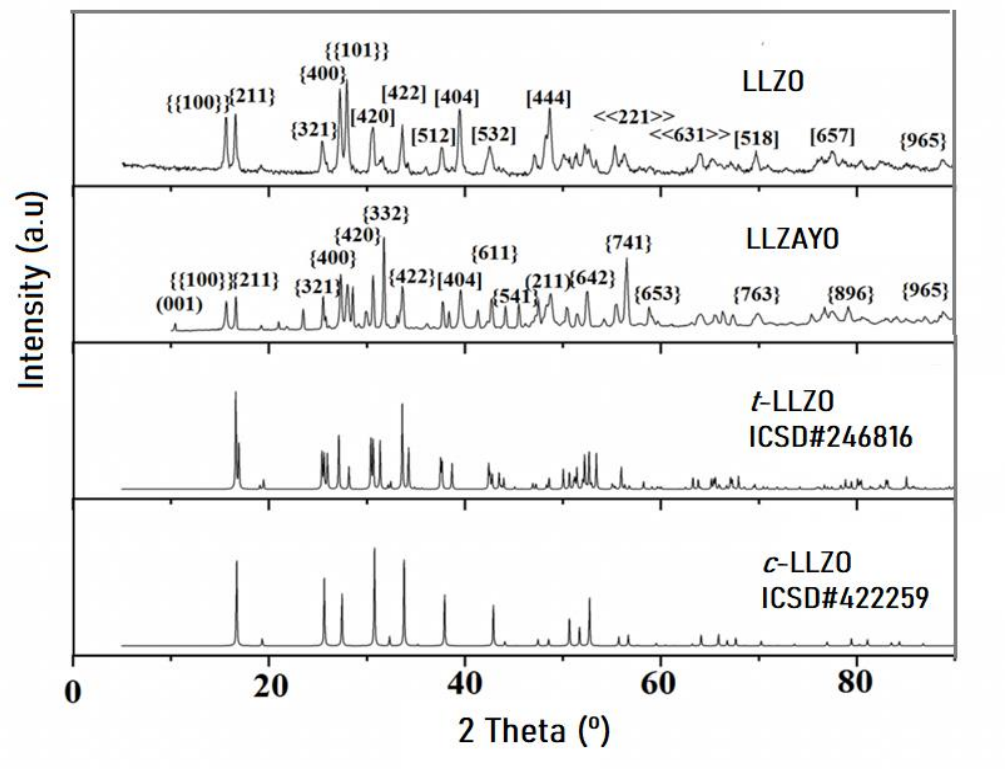

Fig 1. Diffraction patterns of LLZAYO compared with standard diffraction of *c*-LLZO and *t*-LLZO. Cubic diffraction is indexed by { }, tetragonal diffraction is [ ]. Meanwhile, ( ) refers to Y_2O_3 diffraction, and {{ }} refers to $La(OH)_3$.

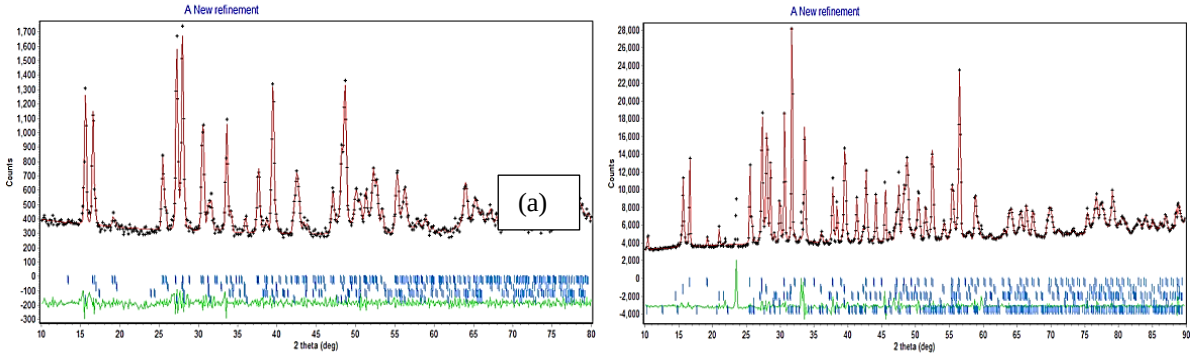

Fig 2. Le Bail plots of (a) LLZO and (b) LLZAYO, black line refers to data, red line is calculation line, blue line is simulated-data, and green line is the difference between data and calculation

single tetragonal phase (Košir *et al*., 2022). Therefore, Al- Y- in this research can quickly transform tetragonal to cubic structure compared with another dopant such as Be-, B-, or Zn (Xiang et al., 2020). However, the purity of the cubic structure needs to be enhanced by eliminating the secondary phases.

Le Bail refinement found that after Al and Y doping, the cubic cell parameter decreased from 13.1(5) Å to 12.98(0) Å. It is possible when a lower ionic radius of Al^{3+} (0.53 Å) replaces Li^+ (0.76 Å), resulting in lithium vacancies to compensate for the excess positive charge, and Al replaces Zr^{4+} (0.79 Å), producing oxygen vacancy for compensation. Meanwhile, when Y^{3+} replaces Zr^{4+} and Li^+, the cell parameter would increase as occurred for the tetragonal *c* cell parameter of 12.7(4)Å, which transformed into cubic *c* of 12.98(0) Å. Defect reaction explains the prediction of Al^{3+} and Y^{3+} doping under an oxygen atmosphere is proposed according to Kröger-Vink Notation (Kingery *et al*., 1977) (Equation 1).

$$Li_7La_3Zr_2O_{12} + Al_2O_3 + Y_2O_3 \rightarrow Al_{Li}^{\bullet\bullet} + Y_{Li}^{\bullet\bullet} + Al_{Zr}' + Y_{Zr}' + Zr_{Zr} + La_{La} + Li_{Li} + 4V_{Li}' + V_O^{\bullet\bullet} + 11O \quad (1)$$

The • sign refers to a positive charge related to the initial charge of the crystal lattice, and V refers to vacancy state that was formed as a compensation of doping. Meanwhile the ′ sign refers to negative charge relatively to the previous state. The ionic conduction of LLZO is supported by the availability of native defect, which are V_{Li}' and $V_O^{\bullet\bullet}$ beside the presence of cation anti sites such as Li_{La}'', La_{Zr}', $Li_{Zr}'''$and $Zr_{Li}^{\bullet}$ (Squires *et al.,* 2020). It seems that the Al- and Y- doping increases the quantity of V_{Li}' (equation (1)). The Al- and Y- doping have changed the electron distribution map of the unit crystal, as it is shown by the Fourier plots (Figure 3) at before doping (Fig. 3(a)) and at after doping (Fig. 3(b)). The Blue line refers to a high electron distribution around a cation site. Fig 3(b) confirms that the presence of Al-

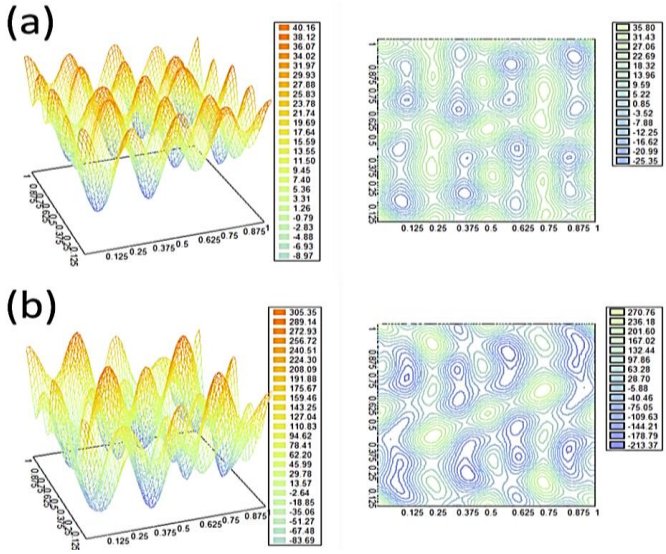

Fig 3. The 3D and 2D Fourier plots of (a) LLZO and (b) LLZAYO. Blue lines indicate high electron distribution, meanwhile, the orange lines refer to lower electron distribution

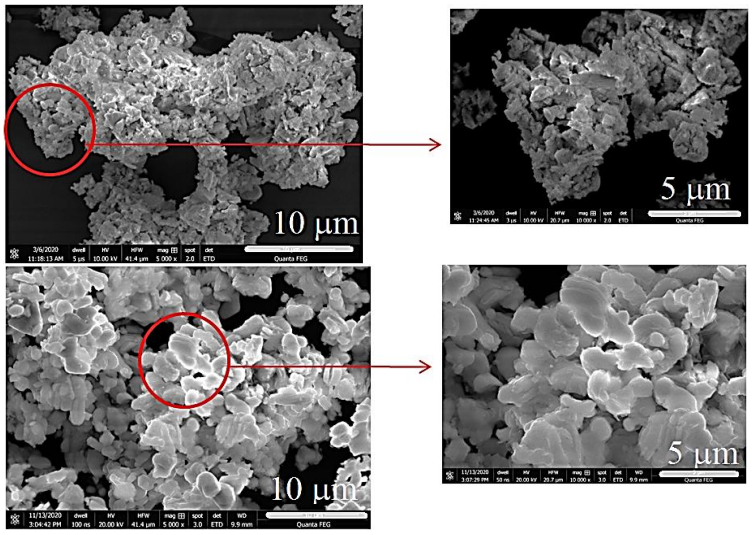

Fig 4. Surface morphology of LLZO (above) and LLZAYO (below)

and Y- connect the lattices by extent the area of electron distribution because of vacancies formation, as shown by a white area in between two sites (Fig 3(b)).

SEM analysis of the prepared LLZO and LLZAYO, as described in Figure 4, shows that both powders are in aggregate with varying sizes and shapes. The grain size of LLZO is 160±50 nm, and LLZAYO is 450±84 nm for LLZAYO. It means that Al- and Y- doping increases the grain size three times larger. The 3+ cation ion of Y and Al trigger exaggerated grain growth resulting large grain size. It also occurred when Ca^{2+} and Ta^{2+} were doped into $Li_{6.6}La_3Zr_{1.6}Ta_{0.4}O_{12}$; some abnormal grain growth is larger than other generated grains (Wang *et al.*, 2021), and when Mn dopant submitted into $(Ba,Sr)TiO_3$ ceramics(Wang *et al.*, 2018).

Cold isostatic pressure was applied to LLZAYO to understand the best pressure for enhancing ionic conductivity. The CIP variation were 0, 20, 30, and 40 MPa. The impedance plots are depicted in Figure 5, and the Zview fitting result is listed in Table 2. Figure 5 shows that the green LLZAYO pellet without CIP treatment has irregular data with a huge semi-circle trend found by ZView fitting, which resulted in a high resistance of (1.09±0.87) x 10^9 Ω (Table 2). The 20 MPa CIP treatment decreases the resistance to 3 orders, then decreases one order up to 40 MPa (Table 2). The resistance decreased about 1.5 times from 30 MPa to 40 MPa. Therefore, increasing pressure to more than 40 MPa will only slightly decrease resistance. The highest ionic conductivity at 40 MPa is (9.06±0.26) x 10^{-6} Scm^{-1},

Table 2
The fitting result by applying R-C network as inserted in Figure 5

materials	Resistance (Ω)	Capacitance (F)	Ionic Conductivity (Scm^{-1})
LLZAYO-CIP0	(1.09± 0.87) x 10^9	(5.98± 2.08) x 10^{-14}	(4.92±4.88) x 10^{-9}
LLZAYO-CIP20	(4.27± 0.63) x 10^6	(4.24±0.07) x 10^{-13}	(5.67±0.78) x 10^{-7}
LLZAYO-CIP30	(4.46±0.19) x 10^5	(1.99± 1.38) x 10^{-11}	(6.30± 0.31) x 10^{-6}
LLZAYO-CIP40	(1.40 ± 0.03) x 10^5	(1.43 ± 0.58) x 10^{-10}	(9.06± 0.26) x 10^{-6}

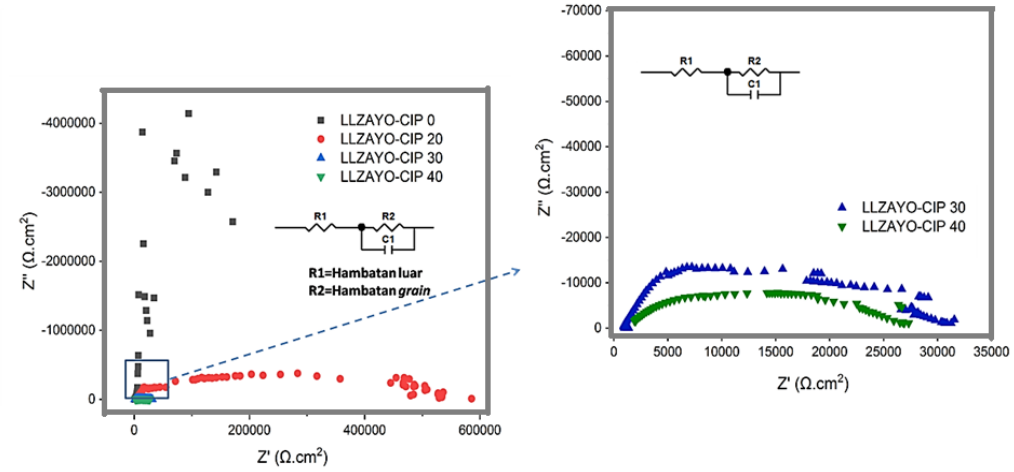

Fig 5. Impedance plots of LLZAYO-CIP0, LLZAYO-CIP20, LLZAYO-CIP30, and LLZAYO-CIP40

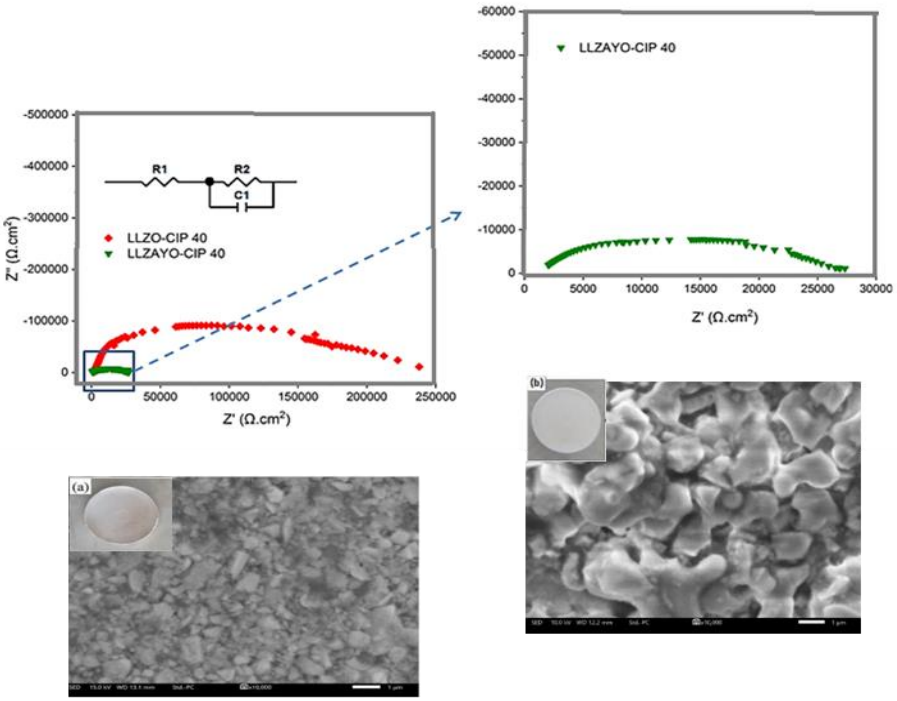

Fig 6. Impedance plots of LLZO CIP-40 and LLZAYO CIP-40 along with its SEM image of (a) LLZO-CIP40 pellet, and (b) LLZAYO-CIP40 pellet. Inserted are optical image of the pellets

which is lower than another result on Ca^{2+} doped-LLZTO (LLZCTO) with the formula of $Li_{6.6+x}La_{3-x}Ca_xZr_{1.6}Ta_{0.4}O_{12}$ that provide s ionic conductivity around 2 x 10^{-4} until 5 x 10^{-4} Scm^{-1}. However, those LLZCTO were heated at 1230 °C 1 h (Wang *et al.*, 2021). Another result on Mo^{2+} doped-LLZO (LLZMO) increases ionic conductivity from 9.14 x 10^{-7} Scm^{-1} for LLZO to 3.17 x 10^{-4} Scm^{-1} after doping. The LLZMO was sintered at 1100 °C for 24 h (Zhou *et al.*, 2022). Therefore, based on this research result and compared with other results, CIP combined with heating treatment can be a good option. A low heating temperature might be sufficient regarding the CIP support for densification. CIP applied isostatic pressure from all directions imposed on the fluid within the mold to dense the green pellet (Zhao *et al.*, 2018).

A similar 40 MPa CIP was applied to LLZO to investigate the advantage of the Al-Y doping into LLZO. The impedance plot of LLZO CIP-40 is depicted in Figure 6, along with their surface morphology and the inserted-optical images. The result is compared with LLZAYO CIP 40, which shows that LLZAYO CIP-40 has lower resistance than LLZO CIP 40. It indicates that Al-Y doping successfully increases the ionic conductivity to about nine times higher. ZView fitting results are depicted in

Table 3
ZView fitting to impedance data of LLZO CIP-40 and LLZAYO CIP-40

Materials	Resistance (Ω)	Capacitance (F)	Ionic Conductivity (Scm^{-1})
LLZO-CIP 40	(1.91± 0.02) x 10^{6}	(1.62± 2.06) x 10^{-11}	(1.25 ± 0.01) x 10^{-6}
LLZAYO-CIP 40	(1.40 ± 0.03) x 10^{5}	(1.43 ± 0.58) x 10^{-10}	(9.06 ± 0.26) x 10^{-6}

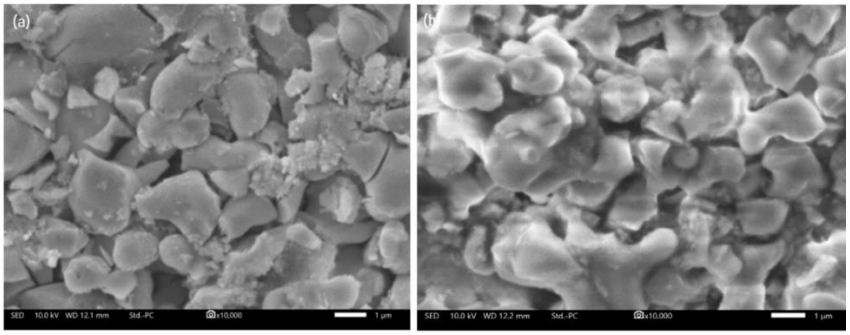

Fig 7. SEM images of (a) LLZAYO green pellet, and (b) LLZAYO-CIP40

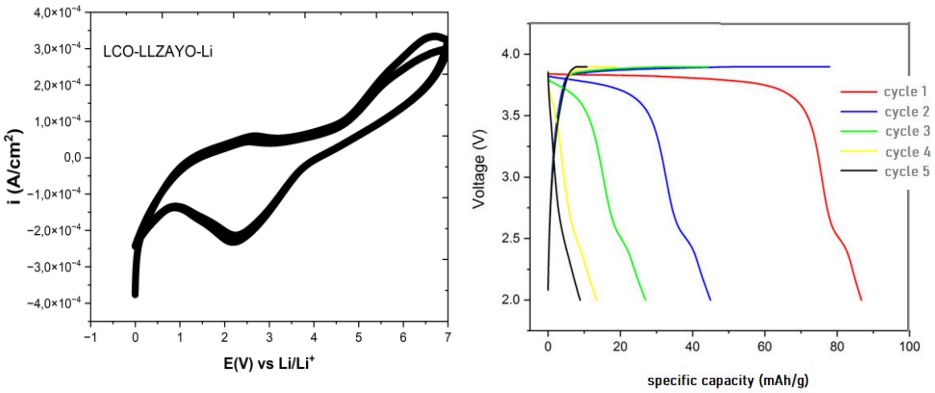

Fig 8. Cyclic voltammogram of LCO-LLZAYO CIP-40-Li at 0 – 7 V vs Li/Li^+ and its charge-discharge profile between 2.0 – 4.0 V at 0.1 mA of current drawn

Table 3, which shows that both LLZO CIP-40 and LLZAYO CIP-40 provide only ionic conduction proven by the capacitance values, which lies at around 10^{-10} to 10^{-11} Farads refers to grain conduction (Martín *et al.,* 2007; Natalia *et al.,* 2019; Rahmawati *et al*., 2019).

SEM images in Figure 6 show that LLZAYO consists of large grains which connect each other after CIP. Meanwhile, LLZO consists of smaller irregular grains without a connection to each other. The CIP effect on LLZAYO is described clearly in Figure 7, in which LLZAYO green pellet consists of irregular size and shape grains, and after CIP treatment, the grains are connected even though there are still some splits between grains. To understand the electrochemical reaction when the solid electrolyte is assembled in a full cell, a prototype of LCO-SE-Li was prepared in a coin cell CR2032 and their cyclic voltammetry was examined. The result shows in Figure 8. Reaction start at around 1.03 V vs. indicates Li to Li+ oxidation, as lithium-ion embedded in a compound usually needs more voltage to oxidize, such as Li in a Li-Hg alloy needs 2.19 V vs SHE for Li oxidation ("APPENDIX H Standard Reduction Potentials," 2022). A second peak revealed at around 4.6 V vs. Li/Li^+ indicates Al oxidation to Al^{3+} (1.66 vs. SHE), which reduced back at around 4.1 V vs. Li/Li^+, along with a second reduction peak at around 0.6 V vs. Li/Li^+. CV analysis shows that the electrochemical reaction within the full cell LCO-LLZAYO CIP40-Li is reversible. However, the redox reaction of Al^{3+} means that the solid electrolyte is electrochemically active, which could cause electronic conduction between anode and cathode and quickly decrease the battery performance, as described in Figure 8. The initial charging capacity was 82 mAh/g, and the initial discharge was 83 mAh/g, confirming 101 % of Coulombic efficiency. However, the discharge capacity drops to 46 mAh/g at cycle-2, leading to a decrease in Coulombic efficiency to 56 %. It seems that LCO is not preferable cathode for LLZAYO, because Co^{3+} reduction potential is much greater than Al^{3+}, which are 1.92 V and -1.676 vs SHE (Libretex, 2023). It implies that Co^{3+} will easily oxidize Al into Al^{3+} when they are in contact during active reaction occurs. Another research uses $LiFePO_4$ to be combined with LLZO based-composite provides better Coulombic effieciency close to 100 % and it was stable until more than 80 cycles (Li et al., 2023). Reduction potential of Fe^{2+} is -0.44 V vs SHE (Libretex, 2023), which is closer to Al^{3+} standard reduction potential. It is essential to find a preferable cathode for this LLAZYO in the future research.

The presence of electronic conduction caused by electrolyte redox reaction is proven by impedance analysis of the full cell of LCO-LLZAYO CIP40-Li before and after five charge-discharge cycles. The impedance plots are depicted in Figure 9, which shows that resistance decreases significantly after the charge-discharge test. ZView fitting analyzes that the resistance consists of ionic and electronic resistance. The electronic resistance is high at the initial condition, i.e., 36622 Ω (Table 4). However, the electrochemically active of the LLZAYO, which was performed by Al redox reaction, decreased the electronic resistance to 1,800 Ω. It means that electrons can transport directly from the anode to the cathode, or a short circuit has occurred, which causes the battery to drop quickly.

4. Conclusion

Dual doping Al- and Y- to lithium lanthanum zirconate, $Li_7La_3Zr_2O_{12}$ transforms the material to crystallize in a single cubic phase. However, the presence of a small number of secondary phases, which are the remaining precursors of La_2O_3 and Y_2O_3 by 0.39 mol% and 12.32 mol%, respectively, indicates that the synthesis method needs a longer time of ball milling. Cold Isostatic Pressing, CIP, could densify the LLZAYO pellet and increase the ionic conductivity to (9.06 ± 0.26) x 10^{-6} Scm^{-1} when 40 MPa of CIP was applied. However, when the solid electrolyte LLZAYO CIP-40 was assembled with $LiCoO_2$

Table 4
ZView fitting result of the LCO-LLZAYO CIP40-Li at before and after 5 cycles charge-discharge

	R_{ionic} (Ω)	C (Farads)	$R_{electronic}$ (Ω)	C(Farads)	Chi-square
Before cycling	126.9	3.72×10^{-10}	36622	2.72×10^{-7}	0.001
After 5 cycles	1783	3.04×10^{-9}	1800	1.04×10^{-6}	0.01

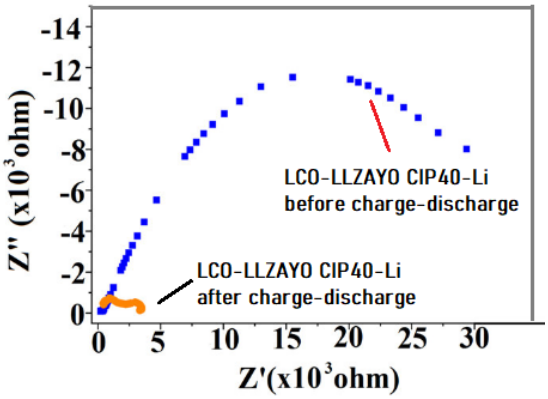

Fig 9. Nyquist plots of LCO-LLZAYO CIP40-Li at before and after 5 cycles charge-discharge

cathode and Li metal anode, Al dopant from LLZAYO underwent a redox reaction which caused the decrease of electronic resistance, or an increase in the electronic conductivity and led to a decrease in the performance of the all-solid-state battery LCO-LLZAYO CIP40-Li.

Acknowledgement

Authors thank The Ministry of Education, Culture, Research, and Technology for funding this research under a scheme of Penelitian Dasar Unggulan Perguruan Tinggi (PDUPT) contract number 221.1/UN27.22/HK.07.00/2021.

References

APPENDIX H Standard Reduction Potentials [WWW Document], 2022. http://www.csun.edu/~hcchm003/321/Ered.pdf(accessed 4.21.23).

Awaka, J., Kijima, N., Hayakawa, H., Akimoto, J., 2009. Synthesis and structure analysis of tetragonal Li7La3Zr2O12 with the garnet-related type structure. *J. Solid State Chem.* https://doi.org/10.1016/j.jssc.2009.05.020

Awaka, J., Takashima, A., Kataoka, K., Kijima, N., Idemoto, Y., Akimoto, J., 2011. Crystal structure of fast lithium-ion-conducting cubic Li 7La3Zr2O12. *Chem. Lett.* 40, 60–62. https://doi.org/10.1246/cl.2011.60

Bernstein, N., Johannes, M.D., Hoang, K., 2012. Origin of the structural phase transition in Li 7La 3Zr 2O 12. Phys. Rev. Lett. https://doi.org/10.1103/PhysRevLett.109.205702

Bitzer, M., Gestel, T. Van, Uhlenbruck, S., Hans-Peter-Buchkremer, 2016. Sol-gel synthesis of thin solid Li7La3Zr2O12 electrolyte films for Li-ion batteries. *Thin Solid Films* 615, 128–134. https://doi.org/10.1016/j.tsf.2016.07.010

Campanella, D., Belanger, D., Paolella, A., 2021. Beyond garnets, phosphates and phosphosulfides solid electrolytes: New ceramic perspectives for all solid lithium metal batteries. *J. Power Sources* 482, 228949. https://doi.org/10.1016/j.jpowsour.2020.228949

Chen, F., Zhang, Y., Hu, Q., Cao, S., Song, S., Lu, X., Shen, Q., 2021. S/MWCNt/LLZO composite electrode with e−/S/Li+ conductive network for all-solid -state Lithium–Sulfur batteries. *J. Solid State Chem.* 301, 122341. https://doi.org/10.1016/j.jssc.2021.122341

Chen, W., Yu, H., Lee, S.Y., Wei, T., Li, J., Fan, Z., 2018. Nanocellulose: a promising nanomaterial for advanced electrochemical energy storage. *Chem. Soc. Rev.* 47, 2837–2872. https://doi.org/10.1039/C7CS00790F

El-Shinawi, H., Paterson, G.W., MacLaren, D.A., Cussen, E.J., Corr, S.A., 2017. Low-temperature densification of Al-doped Li 7 La 3 Zr 2 O 12 : a reliable and controllable synthesis of fast-ion conducting garnets. *J. Mater. Chem. A* 5, 319–329. https://doi.org/10.1039/C6TA06961D

Ghosh, K., Wasim Raja, M., 2022. Ga-Doped LLZO Solid-State Electrolyte with Unique “Plate-like” Morphology Derived from Water Hyacinth (Eichhornia crassipes) Aquatic Weed: Waste to Wealth Conversion. *ACS Omega* 7, 33385–33396. https://doi.org/10.1021/acsomega.2c04012

Hayashi, A., Minami, K., Ujiie, S., Tatsumisago, M., 2010. Preparation and ionic conductivity of Li 7 P 3 S 11 − z glass-ceramic electrolytes. *J. Non. Cryst. Solids* 356, 2670–2673. https://doi.org/10.1016/j.jnoncrysol.2010.04.048

Hung, I.M., Mohanty, D., 2023. Preparation and characterization of LLZO-LATP composite solid electrolyte for solid-state lithium-ion battery. *Solid State Commun.* 364, 115135. https://doi.org/10.1016/j.ssc.2023.115135

Hwang, S., Kim, D.-H., Shin, J.H., Jang, J.E., Ahn, K.H., Lee, C., Lee, H., 2018. Ionic Conduction and Solution Structure in LiPF 6 and LiBF 4 Propylene Carbonate Electrolytes. *J. Phys. Chem. C* 122, 19438–19446. https://doi.org/10.1021/acs.jpcc.8b06035

Inaguma, Y., Seo, A., Katsumata, T., 2004. Synthesis and lithium ion conductivity of cubic deficient perovskites SrLi?TiTaO and the La-doped compounds. *Solid State Ionics* 174, 19–26. https://doi.org/10.1016/j.ssi.2004.06.013

Kim, D.H., Kim, M.Y., Yang, S.H., Ryu, H.M., Jung, H.Y., Ban, H., Park, S., Lim, J.S., Kim, H., 2019. Fabrication and electrochemical characteristics of NCM-based all-solid lithium batteries using nano-grade garnet Al-LLZO powder. *J. Ind. Eng. Chem.* 71, 445–451. https://doi.org/10.1016/j.jiec.2018.12.001

Kingery, W.D., Bowen, H.K., Uhlmann, D.R., Frieser, R., 1977. Introduction to Ceramics. *J. Electrochem. Soc.* 124, 152C-152C. https://doi.org/10.1149/1.2133296

Kokal, I., Somer, M., Notten, P.H.L., Hintzen, H.T., 2011. Sol-gel synthesis and lithium ion conductivity of Li7La 3Zr2O12 with garnet-related type structure. *Solid State Ionics* 185, 42–46. https://doi.org/10.1016/j.ssi.2011.01.002

Li, H.Y., Huang, B., Huang, Z., Wang, C.A., 2019. Enhanced mechanical strength and ionic conductivity of LLZO solid electrolytes by oscillatory pressure sintering. *Ceram. Int.* 45, 18115–18118. https://doi.org/10.1016/j.ceramint.2019.05.241

Li, J., Chang, G., Xu, L., Gao, T., Ma, J., Zhan, D., Lu, X., 2023. EC modified PEO/PVDF-LLZO composite electrolytes for solid state lithium metal batteries. *J. Indian Chem. Soc.* 100, 100959.

https://doi.org/10.1016/j.jics.2023.100959
Li, T., Li, X., Wang, Z., Guo, H., Peng, W., Zeng, K., 2015. Electrochemical properties of LiNi0.6Co0.2Mn0.2O2 as cathode material for Li-ion batteries prepared by ultrasonic spray pyrolysis. *Mater. Lett.* 159, 39–42. https://doi.org/10.1016/j.matlet.2015.06.075
Li, Y., Xu, B., Xu, H., Duan, H., Lü, X., Xin, S., Zhou, W., Xue, L., Fu, G., Manthiram, A., Goodenough, J.B., 2017. Hybrid Polymer/Garnet Electrolyte with a Small Interfacial Resistance for Lithium-Ion Batteries. *Angew. Chemie Int. Ed.* 56, 753–756. https://doi.org/10.1002/anie.201608924
Libretex, C., 2023. P1: Standard Reduction Potentials by Element [WWW Document]. URL https://chem.libretexts.org/Ancillary_Materials/Reference/Reference_Tables/Electrochemistry_Tables/P1%3A_Standard_Reduction_Potentials_by_Element
Martín, P., López, M.L., Pico, C., Veiga, M.L., 2007. Li(4-x)/3Ti(5-2x)/3CrxO4 (0 ≤ x ≤ 0.9) spinels: New negatives for lithium batteries. *Solid State Sci.* 9, 521–526. https://doi.org/10.1016/j.solidstatesciences.2007.03.023
Mizuno, F., Hayashi, A., Tadanaga, K., Tatsumisago, M., 2005. New, Highly Ion-Conductive Crystals Precipitated from Li2S–P2S5 Glasses. *Adv. Mater.* 17, 918–921.
Natalia, V., Rahmawati, F., Wulandari, A., Purwanto, A., 2019. Graphite/Li2ZrO3 anode for a LiFePO4 battery. *Chem. Pap.* 73. https://doi.org/10.1007/s11696-018-0626-0
Priyono, S., Primasari, R.D., Saptari, S.A., Prihandoko, B., 2017. Synthesize Li 4 Ti 5 O 12 from technical grade raw material by excess Li)O.H2O as Anode for Lithium Ion Battery. *J. Physic* 87, 1–6.
Qie, L., Chen, W.M., Wang, Z.H., Shao, Q.G., Li, X., Yuan, L.X., Hu, X.L., Zhang, W.X., Huang, Y.H., 2012. Nitrogen-doped porous carbon nanofiber webs as anodes for lithium ion batteries with a superhigh capacity and rate capability. *Adv. Mater.* 24, 2047–2050. https://doi.org/10.1002/adma.201104634
Rahmawati, F., Zuhrini, N., Nugrahaningtyas, K.D., Arifah, S.K., 2019. Yttria-stabilized zirconia (YSZ) film produced from an aqueous nano-YSZ slurry: preparation and characterization. *J. Mater. Res. Technol.* 1–10. https://doi.org/10.1016/j.jmrt.2019.07.054
Rangasamy, E., Wolfenstine, J., Sakamoto, J., 2012. The role of Al and Li concentration on the formation of cubic garnet solid electrolyte of nominal composition Li 7La 3Zr 2O 12. *Solid State Ionics* 206, 28–32. https://doi.org/10.1016/j.ssi.2011.10.022
Rettenwander, D., Geiger, C.A., Tribus, M., Tropper, P., Amthauer, G., 2014. A Synthesis and Crystal Chemical Study of the Fast Ion Conductor Li7–3xGaxLa3 Zr2O12 with x = 0.08 to 0.84. *Inorg. Chem.* 52, 6264–6269. https://doi.org/10.1021/ic500803h
Takada, K., 2018. Progress in solid electrolytes toward realizing solid-state lithium batteries. *J. Power Sources* 394, 74–85. https://doi.org/10.1016/j.jpowsour.2018.05.003
Wang, C., Lin, P.P., Gong, Y., Liu, Z.G., Lin, T.S., He, P., 2021. Synergistic impacts of Ca2+ and Ta5+ dopants on electrical performance of garnet-type electrolytes. *J. Alloys Compd.* 879, 160420. https://doi.org/10.1016/j.jallcom.2021.160420
Wang, J., Zhao, Y., Shi, X., Zhang, L., 2018. Effect of Mn dopant on the grain size and electrical properties of (Ba, Sr)TiO3 ceramics. J. *Mater. Sci. Mater. Electron.* 29, 11575–11580. https://doi.org/10.1007/s10854-018-9254-2
Xiang, X., Liu, Y., Chen, F., Yang, W., Yang, J., Ma, X., Chen, D., Su, K., Shen, Q., Zhang, L., 2020. Crystal structure and lithium ionic transport behavior of Li site doped Li7La3Zr2O12. *J. Eur. Ceram. Soc.* 40, 3065–3071. https://doi.org/10.1016/j.jeurceramsoc.2020.02.054
Zhao, P., Cao, G., Jin, Z., Ming, H., Wen, Y., Xu, Y., Zhu, X., Xiang, Y., Zhang, S., 2018. Self-consolidation mechanism and its application in the preparation of Al-doped cubic Li7La3Zr2O12. *Mater. Des.* 139, 65–71. https://doi.org/10.1016/j.matdes.2017.10.067
Zhou, X., Huang, L., Elkedim, O., Xie, Y., Luo, Y., Chen, Q., Zhang, Y., Chen, Y., 2022. Sr2+ and Mo6+ co-doped Li7La3Zr2O12 with superior ionic conductivity. *J. Alloys Compd.* 891, 161906. https://doi.org/10.1016/j.jallcom.2021.161906